Phase composition and tribo-mechanical properties of Ti-B-C nanocomposite coatings prepared by magnetron sputtering

J C Sánchez-López[1], M D Abad[1], A Justo[1], R Gago[3], J L Endrino[3,*], A García-Luis[2], M Brizuela[2]

[1]Instituto de Ciencia de Materiales de Sevilla (CSIC-Univ. Sevilla), Avda. Américo Vespucio 49, 41092-Sevilla, Spain.

[2]TECNALIA, MikeleteguiPasealekua 2, 20009 Donostia-San Sebastián, Spain

[3]Instituto de Ciencia de Materiales de Madrid, Consejo Superior de Investigaciones Científicas, 28049 Madrid, Spain

[*] New address: ABENGOA Research S.L., Campus Palmas Altas, 41014 Sevilla, Spain

Abstract

Protective nanocomposite coatings based on hard ceramic phases (TiC, TiB_2) combined with amorphous carbon (a-C) are of interest because of their adequate balance between mechanical and tribological performances. In this work, Ti-B-C nanocomposite coatings were prepared by co-sputtering of graphite and TiB_2 targets. Varying the discharge power ratio applied to the graphite and TiB_2 targets from 0 to 2, the a-C content in the coatings could be tuned from 0 to 60%, as observed by means of Raman and X-ray photoelectron spectroscopy (XPS). The microstructural characterization demonstrated a progressive decrease in crystallinity from an initial nanocrystalline (nc) TiB_2-*like* structure to a distorted TiB_xC_y ternary compound with increasing C concentration. X-ray absorption near-edge structure measurements on the B K-edge helped to determine a hexagonal arrangement around the B atoms in the ternary TiB_xC_y phase. A fitting analysis of the C1s XPS peak allowed to evaluate the relative amount of a-C and TiB_xC_y components. A drastic change in hardness (from 52 to 13 GPa) and friction coefficient

[*]Corresponding author:jcslopez@icmse.csic.es

values (from 0.8 to 0.2) is noticed when moving from nc-TiB_2 to TiBC/a-C nanocomposites. The fraction of a-C necessary to decrease the friction below 0.2 was found to be 45 %. Raman observation of the wear tracks determined the presence of disordered sp^2-bonded carbon phase associated to the diminution of the friction level.

Keywords: TiBC; nanocomposites; wear; hardness; XANES; sputtering; friction

1. Introduction

Nanostructured multiphase composites based upon TiB_2 and TiC or TiN are attractive for the development of new coating materials due to their high hardness, high melting point and their unique functional properties as high wear and corrosion resistance [1-6]. These properties make these composite materials valid candidates as wear-resistant coatings in forming dies and cutting tools [7-13]. Nonetheless, they cannot afford low friction coefficient (namely 0.6 or superior) in unlubricated conditions, especially when compared to diamond-like carbon (DLC) [14] and other carbon containing coatings for which coefficients of friction are approximately 0.1 [15]. They also present brittle properties induced by the ceramic character of their components which makes necessary to reinforce their fracture toughness. In an attempt to improve the friction, wear and toughness properties, the formation of a Ti-B-C nanocomposite mixing hard materials with a ductile phase like amorphous carbon (a-C) is positioned as a good strategy to obtain a blend of good mechanical and tribological performance. Thus, reactive magnetron sputtering from a TiB_2 target with mixtures of argon and different carbon gaseous precursors (C_3H_8 [16] or CH_4 [17]) was firstly investigated. Later works deposited Ti-B-C films by non-reactive sputtering of TiB_2 and C targets [18,19]. X-ray photoelectron spectroscopy (XPS) of the C1s revealed the

existence of a TiB_xC_y phase together with the segregation of a-C that decreased the friction although the hardness was also reduced [19,20]. Alternatively, it has been also considered the possibility of co-sputtering a unique TiC:TiB_2 combined target and a lubricant phase such as graphitic carbon [20-25] or amorphous CN_x phases using Ar/N_2 mixtures [12,13]. These multiphase coatings rendered similar tribological behaviour but maintaining a moderate hardness value of 25-30 GPa, of particular interest for tribological applications. The origin of such behaviour was related to the relative higher contribution of TiB_xC_y and TiC hard phases in a quasi-amorphous or nanocomposite structure [26] or to a multilayer effect, in the case of TiBCN:CN_x coatings [13]. The formation of the ternary TiB_xC_y solid solution was further confirmed by X-ray absorption near edge structure (XANES) studies [27]. This absorption spectroscopy is based on the excitation of electrons from core level shells to empty states giving rise to the observation of some fine structural features related to different bonding environments.

In this paper, we obtain further insight concerning the correlation between the phase composition, chemical bonding and tribomechanical properties by means of a series of Ti-B-C coatings prepared by the most employed approach of TiB_2/graphite targets and later comparison with those previously obtained by these authors using a mixed TiC:TiB_2 target. This study can also be very useful for giving practical advices regarding the optimization of the coating process for specific applications (e.g. hardness for cutting tools or low friction and wear for contact loading surfaces).

2. Materials and methods

The Ti-B-C coatings were prepared by direct current (dc) magnetron sputtering using a CemeCon® CC800/8 PVD equipment with four rectangular magnetrons (200

mm x 88 mm x 5 mm) in an Ar atmosphere (0.5 Pa; 220 sccm). The deposition process started with resistive heating of the chamber to reach a base pressure below 1×10^{-6} Pa, followed by a plasma etching of the substrates in Ar at −200 V r.f. bias voltage. During the coating process, a dc bias of -65 V was applied to the substrate and the temperature on the sample holder was found to be 350 ºC. Two TiB_2 targets (set at 1750 W of sputtering power, P_{TiB_2}) and two graphite targets (sputtering power, P_C, from 0 to 3300 W) were installed for the experiments. The thicknesses of the coating span between 3.5 and 8 μm. The parameter used to control the carbon content in the coatings was the relative sputtering power ratio (R), defined as the ratio of sputtering power applied to the graphite target in relation to the TiB_2 target (i.e. P_C/P_{TiB_2}). All the coatings were deposited on Si (100) and hardened AISI M2 steel discs of 45 mm diameter and 5 mm thick with a surface finish of 0.01 mm Ra. The tempering process of the M2 substrates was done at 700-850ºC (preheating), 1200ºC (quenching) and 560ºC (tempering) to give a final hardness of 65 HRc.

The crystal structure of the films was examined by grazing incidence X-ray diffraction (XRD) using an angle of 1º and Cu Kα radiation in a Siemens D5000 diffractometer. A JEOL JXA-8200 electron probe microanalysis (EPMA) instrument was used to determine the chemical composition. Raman spectra measurements (200-2000 cm^{-1}) were carried out with a LabRAM (from Horiba Jobin Yvon) spectrometer equipped with a charge-coupled device detector and a He-Ne laser (532 nm) at 5 mW. All the samples were analyzed with 100 s exposure times and aperture openings of 100 μm. XANES B K-edge spectra were collected using the Variable Line Spacing Plane Grating Monochromator (VLS PGM, 11ID-2) at the Canadian Light Source (CLS) synchrotron. Bulk-sensitive total fluorescence yield (TFY) data were recorded using a two-stage multichannel plate detector with the sample surface positioned approximately

80º with respect to the incident X-ray beam. XPS measurements were carried out using a Leybold-Heraeus spectrometer equipped with an EA-200 hemispherical electron multichannel analyzer, operating with a non-monochromated Mg K_α X-ray source (1253.6 eV). A five-minute Ar^+ sputtering at a voltage of 3 kV and a pressure of 2×10^{-6} Pa was carried out in order to remove the surface contamination and oxidation. Fitting analysis was performed on the C 1s peak in order to estimate the relative amount of the different carbon bonds (carbides and amorphous carbon). Data fitting was carried out by a least squares routine supplied by XPS Peak Fitting Programme 4.1 [28], using mixed Gaussian-Lorentzian peaks following a Shirley background subtraction.

The mechanical properties were measured on coated AISI M2 steel disks with a Fischercope H100 dynamic microprobe instrument using a conventional Vickers indenter, at loads up to 10 mN. The maximum load was selected in such a way that the maximum indentation depth did not exceed 10-15% of the coating thickness, thus avoiding the influence of the substrate in the measurement. The test parameters were fixed to an initial load of 0.4 mN, increasing to a maximum load of 10 mN in 40 load steps, with a 0.5 s interval between loading steps. The hardness and reduced Young's modulus were calculated from the load-unload displacement curves. The tribological properties of the coatings were evaluated on coated M2 steel disks by ball-on-disk friction tests in unlubricated sliding against WC or 100Cr6 steel 6-mm balls in ambient air, with relative humidity between 40-50%. The test parameters were set to an applied load of 1N for the WC balls and 5N for the steel balls (corresponding to a similar maximum initial Hertzian contact pressure of around 1GPa), a linear speed of 10 cm/s, and a sliding distance of 1000 m. Normalized wear rates (mm^3/Nm) were evaluated from cross-sectional profiles taken across the disk-wear track using stylus profilometry.

3. Results and discussion

3.1. Chemical and structural characterization

The chemical composition of the Ti-B-C coatings as determined by EPMA is summarized in Table 1. Oxygen contamination was found in the level of 0-5 at. %, increasing with the incorporation of carbon. The influence of the sputtering power ratio is revealed by a continuous increment of the C content at an approximate constant ratio B/Ti. These results are in agreement with previously published results on Ti-B-C coatings using a similar target configuration following the tie-line of TiB_2-C of a Ti-B-C phase diagram [1,7,19,29,30].

XRD patterns collected from the six coatings are shown comparatively in Fig. 1. The position of the main diffraction peaks for TiB_2 and TiC phases are marked in the graph for comparison. The first coating prepared by single sputtering of the TiB_2 target exhibits a diffraction pattern in agreement with a hexagonal TiB_2–like structure. Later, with the progressive incorporation of carbon into the coatings, the peaks become broader and less intense. Focussing in the (001) peak, the next sample (R0.5 with 22 at.% of C) exhibits two components with higher and lower spacing than that of pure TiB_2. The higher lattice spacing (i.e., lower 2θ values) is probably caused by the interstitial solid-solution of carbon atoms in the TiB_2 crystal cell whilst the lower spacing can be explained by substitutional carbon in the TiB_2 hexagonal layers forming a ternary TiB_xC_y phase. The lower atomic radius of carbon (0.77 Å) in respect of boron atoms (0.97Å) is responsible of the lattice contraction. The formation of a ternary TiB_xC_y compound has been previously proposed by Knotek and others

[17,18,23,27,31], although other authors suggest the formation of mixture of quasi-amorphous TiC and TiB_2 phases [7]. The remaining samples show preferentially this TiB_xC_y peak with a marked reduction of the average crystallite size. This fact is in agreement with the decrease of boron concentrations with respect to carbon, particularly above R1, favouring the replacement of the former atoms by the latter ones.

Figure 2 shows the B K-edge XANES spectra for the set of the Ti-B-C films and three references for bulk microcrystalline TiB_2, cubic and hexagonal ternary TiB_xC_y phases. The spectra of the samples with the lowest C contents (R0 and R0.5) differ noteworthy from the remaining ones indicating a drastic structural change for carbon contents above 30 at. %. Such trend is in agreement with the deterioration of the crystalline order and change of phase composition assessed by XRD (cf. Fig. 1). Several features appear in the 190-195 eV region of the B K-edge spectra displayed in Fig. 2 that provide information about the local-arrangements of B sites within the compound. The first peak at 190.6 eV (B1) can be assigned to B atoms in hexagonal configuration as present in the TiB_2 reference. This feature is dominant for C < 30 at. % and decreases for larger C contents due to the deterioration of the nc-TiB_2 structure. As expected from the XRD pattern in Fig. 1, the spectra of the R0.5 sample resembles that obtained by sputtering of the TiB_2 target (R0). When the carbon content overcomes 30 at.% a new peak at 192.9 eV (B3) becomes dominant. This peak can be related to boron atoms in a hexagonal ternary TiB_xC_y compound as compared to the reference spectrum [27]. The intensity of this peak manifests an increment at the expense of B1, indicating an evolution of the hexagonal structure from nc-TiB_2-like to short-range arrangements in a disordered ternary h-TiB_xC_y phase. This peak becomes dominant at higher carbon contents confirming the hypothesis of a certain incorporation of carbon atoms inside the lattice of TiB_2 and formation of a hexagonal ternary (disordered) compound, as

proposed by many authors [17,18,21], instead of a mixture of nc-TiB_2 in a quasi-amorphous TiC phase [7]. Interestingly, the formation of cubic TiB_xC_y arrangements reported in [27] when using a mixed TiB_2/TiC target is not observed in the present work (cf. reference c-TiBC). Such phase was identified with a characteristic feature around 192.4 eV. This result implies that phase formation in the Ti-B-C system is not only driven by compositional issues but can also be tuned by specific conditions such as the appropriate selection of the sputtering targets. A small contribution appears in some of the spectra at 194.3 eV (B4) due to B-O formation since its position matches that of B_2O_3 [32]. As commented before, we noted a slight oxygen contamination within the sample increasing with the C content.

Fig. 3 depicts the Raman spectra for the as-deposited coatings. The spectra were measured in identical conditions to allow a direct comparison of their intensities. The presence of the D and G peaks at 1350 and 1585 cm^{-1} respectively, characteristic of the sp^2 sites of all disordered carbons [33], is more significant when increasing the carbon content inside the coating. Nevertheless there are differences regarding the onset of development and definition of the D and G peaks. Thus, the Ti-B-C coatings with less carbon content, up to 22 at.% of C, do not show evidences of segregated a-C. Beyond this point the peaks are better defined exhibiting a progressive increase in intensity and downward shift of the D peak. This result correlates with the noticeable decrease in the crystallinity observed by XRD. Once the solubility of carbon inside the TiB_2 lattice is reached, either in substitutional or interstitial sites, the further addition of C atoms yields the formation of a disordered a-C phase that surrounds the TiB_xC_y nanocrystals. It is therefore important to determine the distribution of the carbon atoms in this chemical state as the mechanical and tribological performance can be directly

influenced by them. In order to assess this fraction XPS analysis was performed on the C1s peak following the same procedure as reported previously [20,26].

Fig. 4a shows the C 1s photoelectron spectra for the coatings with C content above 22 at. %, when the presence of a disordered C-C phase was noticed. Basically, three main components can be considered at 283.2, 284.5 and 286.0 eV corresponding to typical binding energies of C in TiB_xC_y, sp^2 C-C and C-OH bonds respectively. No peak was clearly detected at 282.0 eV for Ti-C bonding. A gradual shift of the main peak towards the value characteristic of the C-C phase is observed as the concentration of C increases. In order to obtain a more quantitative insight of the compositional changes a fitting analysis was carried out. Fig 4b shows the fitted C 1s XPS peaks after Ar^+ bombardment for the sample containing 34 at.% as a representative example.We define the fraction of the different bonding types, x_i (%), as the fraction of a specific type of carbon bonding in respect to the total carbon content. The obtained values are plotted in Fig. 5. A continuous decrease of the $x_{TiB_xC_y}$ (especially above R1) is observed with the increment of the carbon content. The $x_{a\text{-}C}$ becomes comparable or even higher for the richest C contents. The estimation of the phases present in the nanocomposite will be very useful to obtain correlation with the tribomechanical properties as shown in the next section.

3.2. Tribo-mechanical characterization

Figure 6 shows the tribological results (friction coefficient and film wear rate) for the six coatings using steel balls (Fig. 6a) and WC balls (Fig. 6b) as counterface materials. The hardness values are also superimposed on the same bar-chart showing a marked decreasing trend, from 52 to 13 GPa as the power ratio increases. The

tribological behaviour is very similar independently of the nature of the counterpart displaying lower friction coefficient and wear rates as the carbon content is increased. Note that the worn track profile in R0 was not possible to be measured due to material transfer from the steel ball. Considering the relative amount of a-C ($x_{a\text{-}C}$) estimated previously by XPS, we can re-plot the tribomechanical properties as a function of this parameter. Figure 7 shows the obtained graph using the tests made with WC balls as representative example. It can be noticed the separation of the samples into two main categories corresponding to pure nc-TiB_2 and TiB_xC_y/a-C nanocomposites. The hardness reaches a maximum value of 52 GPa for the nanocrystalline TiB_2 coating as corresponds to its high ceramic nature. When the a-C content increases, both the friction coefficient and film wear rates diminish continuously. The friction coefficient can be reduced below 0.2 when the $x_{a\text{-}C}$ overcomes 45%. This tribological behaviour agrees with that typically observed in carbon-based lubricant nanocomposite coatings [14,15]. The a-C phase is able to accommodate sliding motion, decreasing the shear strength and wear as it comes out from the coating. In comparison with previous TiBC/a-C coatings obtained by some of the present authors using a compound target of TiC:TiB_2 [26,27], the tribological and mechanical properties are worsened at a comparable fraction of a-C. The origin must be found in the different phases present in the composite. Thus, while co-sputtering from TiB_2 and graphite targets only promoted the formation of hexagonal ternary TiB_xC_y compounds, the combination of mixed TiC:TiB_2 and graphite targets promotes the formation of TiC_{1-x} and cubic TiB_xC_y hard phases maintaining higher average hardness values [27]. This is also consistent with the TiB_2-TiC-C phase diagram; the first route produces coatings varying their composition along the TiB_2-C tie-line while the coatings prepared by the second one are inside the region where the three phases (two hard and one soft) can coexist. This might explain the increment of

the film wear rate resistance by a factor of three in the case of a mixed TiC:TiB_2 target. In addition, for achieving a low friction coefficient (i.e. 0.2), less amount of $x_{a\text{-}C}$ is needed (between 15-20%) what helps to maintain an average higher hardness as the contribution of the soft lubricant phase is lower. In conclusion, the co-sputtering of graphite with a mixed TiC:TiB_2 target is more efficient than combining with a TiB_2 target for preparing tribological TiBC/a-C nanocomposites. Nevertheless, if we are seeking for extremely hard coatings without requirements of lubricant behaviour, the sputtering route (TiB_2/C) is more appropriate because of the formation of nanocrystalline TiB_2 with superhardness properties (52 GPa).

A deeper investigation of the friction mechanism was carried out by Raman spectroscopy analysis on the ball scars for representative coatings exhibiting friction coefficient of 0.8, 0.4 and 0.2. Fig. 8 depicts the Raman spectra obtained from the ball scars (steel and WC) for the coatings R0, R1 and R1.9 with $x_{a\text{-}C}$ percentages of 0, 25 and 62% respectively. The optical micrographs obtained from the steel balls are shown as example to illustrate the increment of the worn volume as the fraction of lubricant a-C phase decreases in the coating. In the high friction regime (0.8), the Raman spectra taken from the material adhered to the ball did not show the characteristics D and G bands of disordered sp^2 carbon structures that appear clearly identified in the other cases. In this case, the presence of iron and tungsten oxides is predominant. Particularly, a higher reactivity is noticed in the case of the 100Cr6 ball where a mixture of α-Fe_2O_3, Fe_2O_3 and Fe_3O_4 compounds is identified. This is in agreement with the transfer of ball material to the film counterface observed with the R0 sample, the hardest film without a-C fraction. For the WC balls, several broad bands appear below 800 cm^{-1} that can be related to W–O–W bending modes (in the range of 200–400 cm^{-1}) and W–O-W stretching modes (600–900 cm^{-1}) of disordered tungsten oxides [34-36]. The presence

of mixed boron or titanium oxides cannot be totally discarded. The formation of graphitic-like structures in the contact appears associated to the decrease of the friction coefficient as seen previously in many nanocomposites and carbon-based solid lubricants [14,15,37-39]. It is also manifested a sharpening of the D and G peaks as compared to the initial state.

4. Conclusions

Protective Ti-B-C coatings based on the combination of hard ternary phases (TiB_xC_y) and a-C were prepared by magnetron co-sputtering technology using the combination of TiB_2 and graphite targets. The obtained series of coatings manifested differences in the structural evolution, chemical bonding and tribo-mechanical properties as the carbon content increased. Thus, the film structure evolves from nc-TiB_2 to nanocomposite TiBC/a-C. In the nanocomposite films, a ternary TiB_xC_y compound with a hexagonal arrangement was assessed by XANES analysis of the B K-edge, indicating the replacement of boron by carbon atoms in the TiB_2 lattice. Concerning the tribological properties, the friction mechanism is controlled by the relative amount of a-C phase formed in the contact, as demonstrated by estimation of the $x_{a\text{-}C}$ and Raman study of the worn surfaces. When there is sufficient lubricant a-C (approximately $x_{a\text{-}C} > 45\%$) the friction coefficient and film wear rates were reduced to 0.2 and 10^{-6} mm^3/Nm, respectively. However, a comparison with homologous TiBC/a-C nanocomposites prepared by co-sputtering from a mixed TiC:TiB_2 and graphite targets showed better wear resistance, probably linked to the formation of cubic TiB_xC_y and TiC_{1-x} compounds, with resulting improved mechanical properties. The appropriate selection of the nature of the target composition used for the PVD process is revealed as an

important factor to consider to tune the final properties of a specific coating material for a selected application since it has a direct influence on the type of chemical bonding present in the films and their properties as a result.

Acknowledgements

The Spanish MEC (projects nº MAT2007-66881-C02-01/-02, MAT2011-29074-C02-01/-02, FIS2009-12964-C05-04 and CONSOLIDER FUNCOAT CSD2008-00023), and Junta de Andalucía P10-TEP-6782 are acknowledged for financial support. The research performed at the Canadian Light Source is supported by the Natural Sciences and Engineering Research Council of Canada, the National Research Council Canada, the Canadian Institutes of Health Research, the Province of Saskatchewan, Western Economic Diversification Canada, and the University of Saskatchewan. Dr. Lucia Zuin, VLS PGM beamline scientist, is also acknowledged for her support in the XANES measurements.

References

[1] Holleck H, Lahres M 1991 *Mat. Sci. Eng.* **140** 609-15.

[2] Mollart T P, Baker M, Haupt J, Steiner A, Hammer P, Gissler W 1995 *Surf. Coat. Technol.* **74-75** 491-6.

[3] Wiedemann R, Weihnacht V, Oettel H 1999 *Surf. Coat. Technol.* **116–119** 302-9.

[4] Berger M, Karlsson L, Larson M, Hogmark S 2001 *Thin Solid Films* **401** 179-86.

[5] Kustas F, Mishra B, Zhou J 2002 *Surf. Coat. Technol.* **153** 25-30.

[6] Vallauri D, Atías Adrián I C, Chrysanthou A 2008 *J. Eur. Ceram. Soc.* **28** 1697-1713.

[7] Mitterer C, Mayrhofer P H, Beschliesser M, Losbichler P, Warbichler P, Hofer F, Gibson P N, Gissler W, Hruby H, Musil J, Vlček J 1999 *Surf. Coat. Technol.* **120-121** 405-11.

[8] Mayrhofer P H, Mitterer C 2000 *Surf. Coat. Technol.* **133-134** 131-7.

[9] Prakash B, Richter E, Pattyn H, Celis J P 2003 *Surf. Coat. Technol.* **173** 150-60.

[10] Zhong D, Moore J J, Mishra B M, Ohno T, Levashov E A, Disam J 2003 *Surf. Coat. Technol.***163-164** 50-6.

[11] García-Luis A, Brizuela M, Oñate I, Sánchez-López J C, Martínez-Martínez D, López-Cartes C, Fernández A 2005 *Surf. Coat. Technol.* **200** 734-8.

[12] Vyas A, Lu Y H, Shen Y G 2010 *Surf. Coat. Technol.* **204** 1528-34.

[13] Lin J, Moore J J, Pinkas M, Zhong D, Sproul W 2011 *Surf. Coat. Technol.* **206** 617-22.

[14] Sánchez-López J C, Fernández A, Doping and Alloying Effects on DLC coatings, in: Erdemir A, Donnet C (Eds.) 2008 Tribology of Diamond-Like Carbon Films: Fundamentals and Applications. Springer, New York, pp 311-38.

[15] Sánchez-López J C, Martínez-Martínez D, López-Cartes C, Fernández-Ramos C, Fernández A 2005 *Surf. Coat. Technol*. **200** 40-5.

[16] Mitterer C, Rauter M, Rödhammer P 1990 *Surf. Coat. Technol.* **41** 351-63.

[17] Knotek O, Breidenbach R, Jungblut F, Löffler F 1990 *Surf. Coat. Technol.* **43-44** 107-15.

[18] Stüber M, Schier V, Holleck H 1995 *Surf. Coat. Technol.* **74-75** 833-37.

[19] Gilmore R, Baker M A, Gibson P N, Gissler W 1998 *Surf. Coat. Technol.* **105** 45-50.

[20] Abad M D, Sánchez-López J C, Brizuela M, García-Luis A, Shtansky D V (2010) *Thin Solid Films* **518** 5546-52.

[21] Zhong D, Sutter E, Moore J J, Mustoe G G W, Levashov E A, Disam J 2001 *Thin Solid Films* **398–399** 320-25.

[22] Levashov E A, Kosayanin V I, Krukova L M, Moore J J, Olson D L 1997 *Surf. Coat. Technol.* **92** 34-41.

[23] Park I W, Kim K H, Kunrath A O, Zhong D, Moore J J, Voevodin A A, Levashov E A 2005 *J. Vac. Sci. Technol. B* **23** 588-93.

[24] Lin J, Moore J J, Mishra B, Pinkas M, Sproul W D 2010 *Acta Mater.* **58** 1554-64.

[25] Lin J, Mishra B, Moore J J, Pinkas M, Sproul W D 2008 *Surf. Coat. Technol.* **203** 588-93.

[26] Abad M D, Cáceres D, Pogozhev Y S, Shtansky D V, Sánchez-López J C 2009 *Plasma Process Polym.* **6** S107-12.

[27] Abad M D, Sanjinés R, Endrino J L, Gago R, Andersson J, Sánchez-López J C 2011 *Plasma Process Polym.* **8** 579-88.

[28] Kwok R W M, XPS Peak Fitting Program for WIN95/98 XPSPEAK Version 4.1, Department of Chemistry, The Chinese University of Hong Kong, 2000.

[29] Baker M A 2007 *Surf. Coat. Technol.* **201** 6105-11.

[30] Gorokhovsky V, Bowman C, Gannon P, Van Vorous D, Voevodin A A, Rutkowski A, Muratore C, Smith R J, Kayani A, Gelles D, Shutthanandan V, Trusov B G 2006 *Surf. Coat. Technol.* **201** 3732-47.

[31] Endrino J L, Abad M D, Gago R, Horwat D, Jiménez I, Sánchez-López J C 2010 *IOP Conf. Ser.: Mater. Sci. Eng.* **12** 012012.

[32] Jia J J, Underwood J H, Gullikson E M, Callcott T A, Perera R C C 1996 J. Elec. Spec. Relat. Phenom. **80** 509-12

[33] Ferrari A C, Robertson J 2000 *J. Phys. Rev. B* **61** 14095-107.

[34] Baserga A, Russo V, Di Fonzo F, Bailini A, Cattaneo D, Casari C S, Li Bassi A, Bottani C E 2007 *Thin Solid Films* **515** 6465-69.

[35] Yang B Q, Wang X P, Zhang H X, Wang Z B, Feng P X 2008 *Mater. Lett.* **62** 1547-50.

[36] El Mrabet S, Abad M D, López-Cartes C, Martínez-Martínez D, Sánchez-López J C 2009 *Plasma Process Polym.* **6** S444-49.

[37] Sánchez-López J C, Martínez-Martínez D, Abad M D, Fernández A 2009 *Surf. Coat.Technol.* **204** 947-54.

[38] Martínez-Martínez D, López-Cartes C, Justo A, Fernández A, Sánchez-López J C 2009 *Solid State Sciences* **11** 660-70.

[39] Abad M D, Muñoz-Márquez M A, El Mrabet S, Justo A, Sánchez-López J C 2010 *Surf. Coat. Technol.* **204** 3490-500.

Figure captions

Fig. 1.Grazing angle X-ray diffraction patterns of Ti-B-C coatings deposited onto M2 steel substrates. The reflections from references of TiC (JCPDS Nr: 32-1383) and TiB_2 (075-0967) materials are included for comparison.

Fig. 2. B-K XANES spectra for the Ti-B-C films at five different synthesis conditions. The spectra for cubic and hexagonal TiB_xC_y structures together with a microcrystalline TiB_2 powder from Sigma-Aldrich are included for comparison.

Fig. 3.Raman spectra for the Ti-B-C coatings as a function of the sputtering conditions and total carbon content.

Fig. 4.(a) XPS spectra in the C 1 s region for Ti-B-C films under study as a function of the carbon content. (b) Curve fitted XPS C1s peak for the sample R1.3 as representative example.

Fig. 5. Relative amount of the different carbon-containing phases x_i (%) as a function of the total carbon content.

Fig. 6.Tribological properties of the Ti-B-C coatings using 100Cr6 steel (a) or WC (b) balls as antagonist materials. The measured hardness values are superimposed in the same graph.

Fig. 7. Dependence of the tribo-mechanical properties of the Ti-B-C coatings vs. WC balls with the relative fraction of amorphous carbon phase.

Fig.8. Raman analysis of the worn ball surfaces corresponding to samples R0, R1 and R1.9: (a) steel balls; (b) WC balls. The optical micrographs corresponding to the scars obtained on the steel balls are included as example.

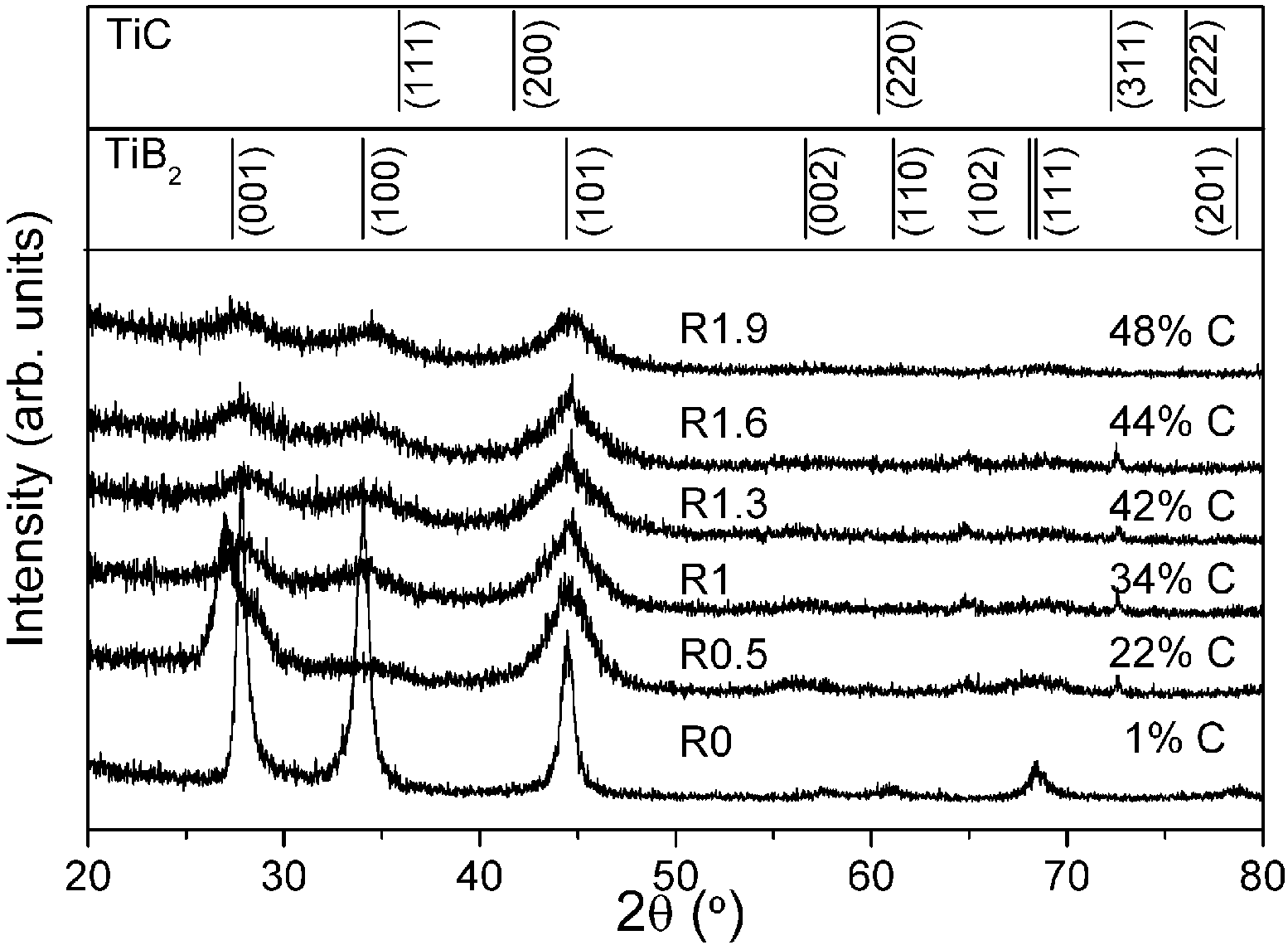
TiC
(111)
(200)
(220)
(311)
(222)
TiB2
(001)
(100)
(101)
(002)
(110)
(102)
(111)
(201)
R1.9
48% C
R1.6
44% C
R1.3
42% C
R1
34% C
R0.5
22% C
R0
1% C
Intensity (arb. units)
20
30
40
50
60
70
80
2θ (°)

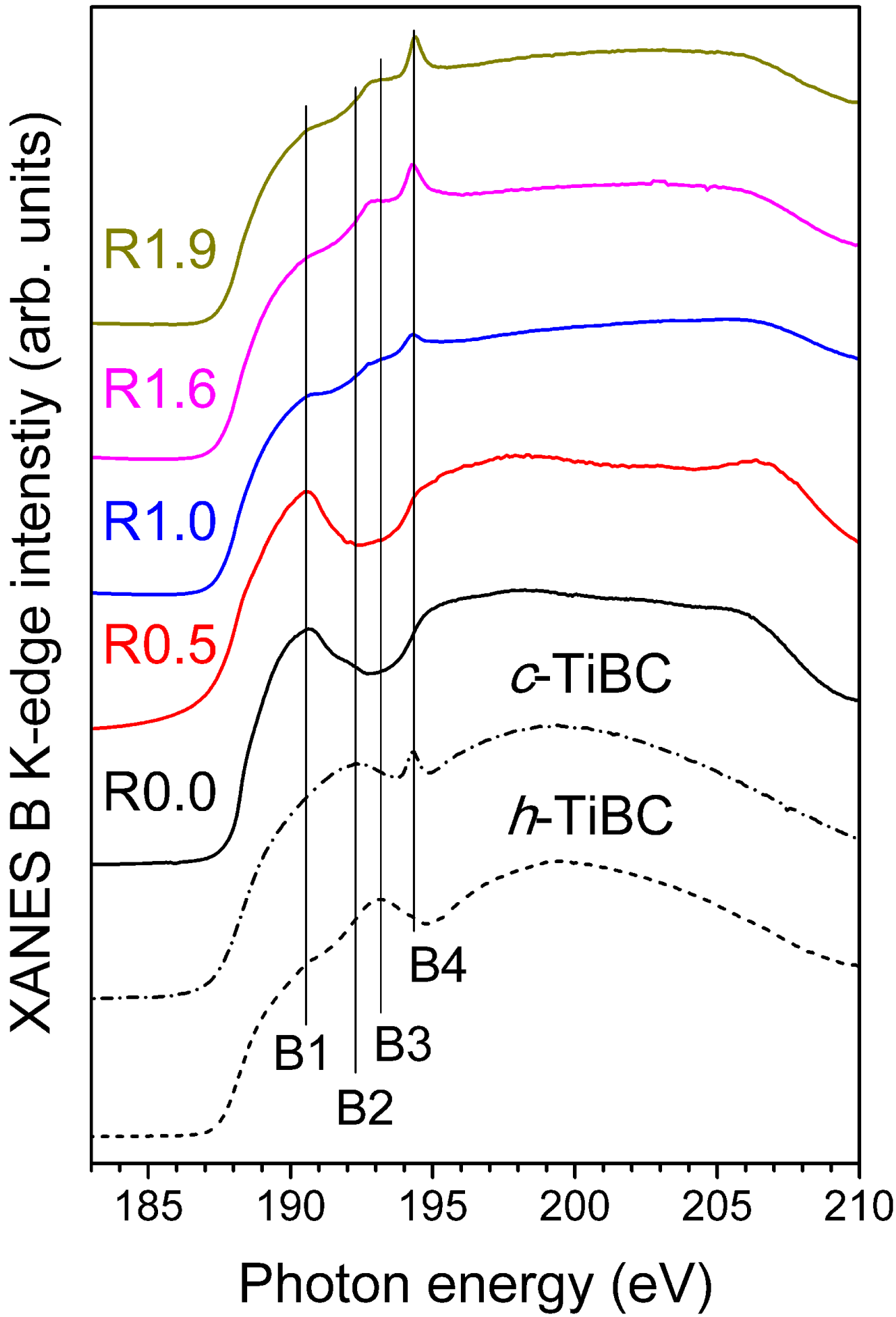
XANES B K-edge intenstiy (arb. units)
R1.9
R1.6
R1.0
R0.5
R0.0
c-TiBC
h-TiBC
B1
B2
B3
B4
185
190
195
200
205
210
Photon energy (eV)

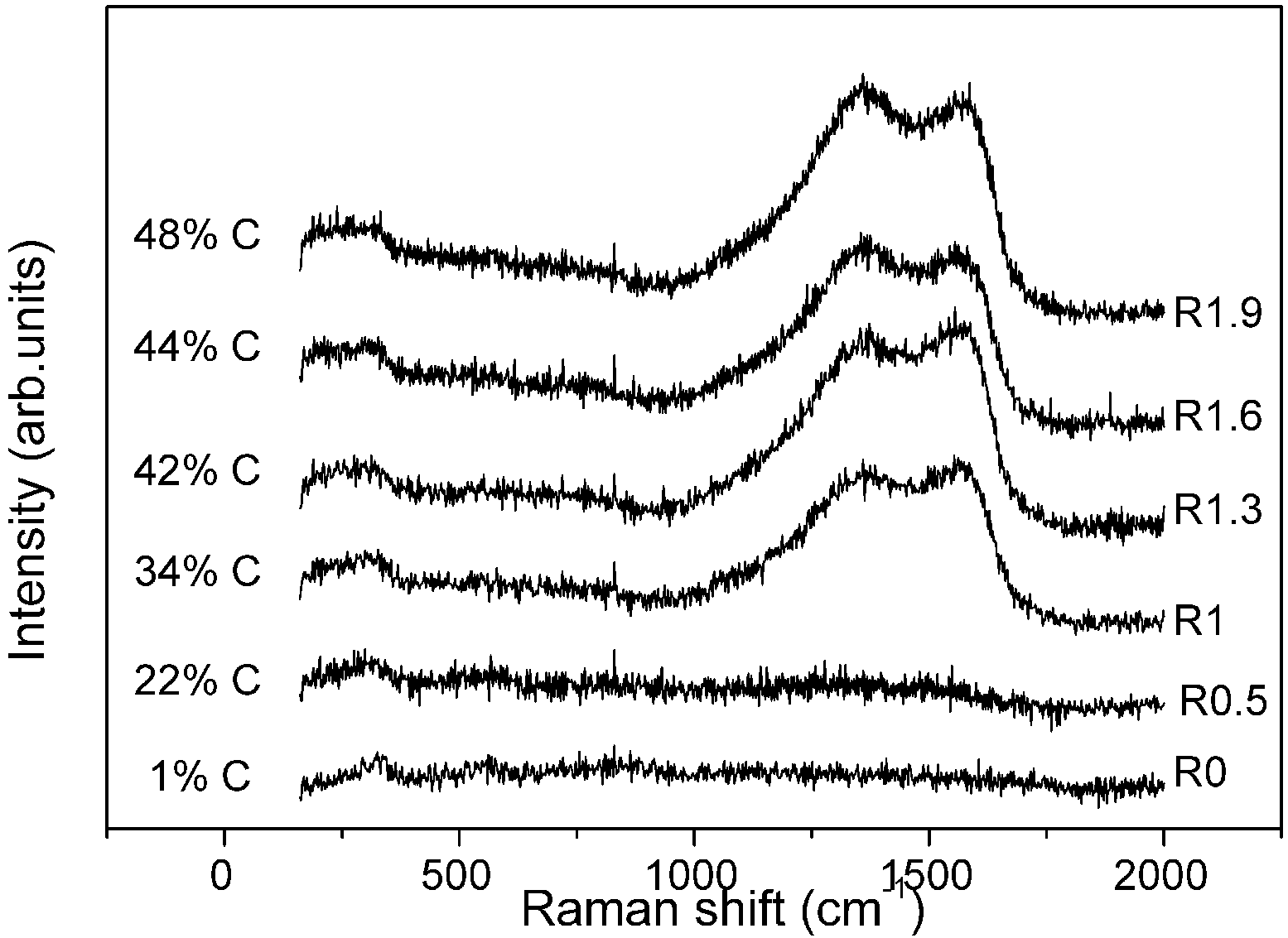
Intensity (arb.units)
48% C
44% C
42% C
34% C
22% C
1% C
R1.9
R1.6
R1.3
R1
R0.5
R0
0
500
1000
1500
2000
Raman shift (cm-1)

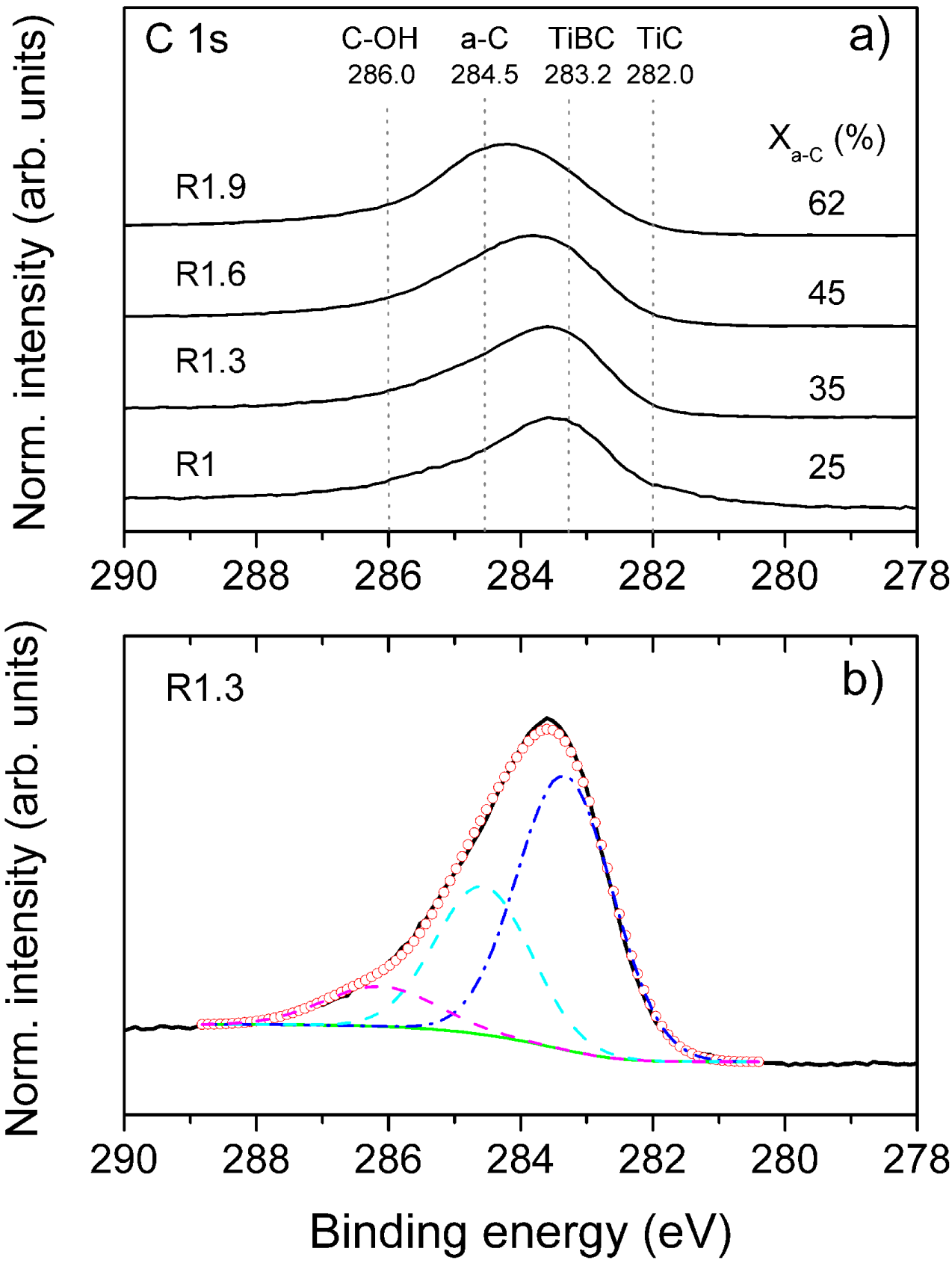
C 1s
C-OH
286.0
a-C
284.5
TiBC
283.2
TiC
282.0
a)
X_{a-C} (%)
R1.9
62
R1.6
45
R1.3
35
R1
25
Norm. intensity (arb. units)
290
288
286
284
282
280
278
R1.3
b)
Norm. intensity (arb. units)
290
288
286
284
282
280
278
Binding energy (eV)

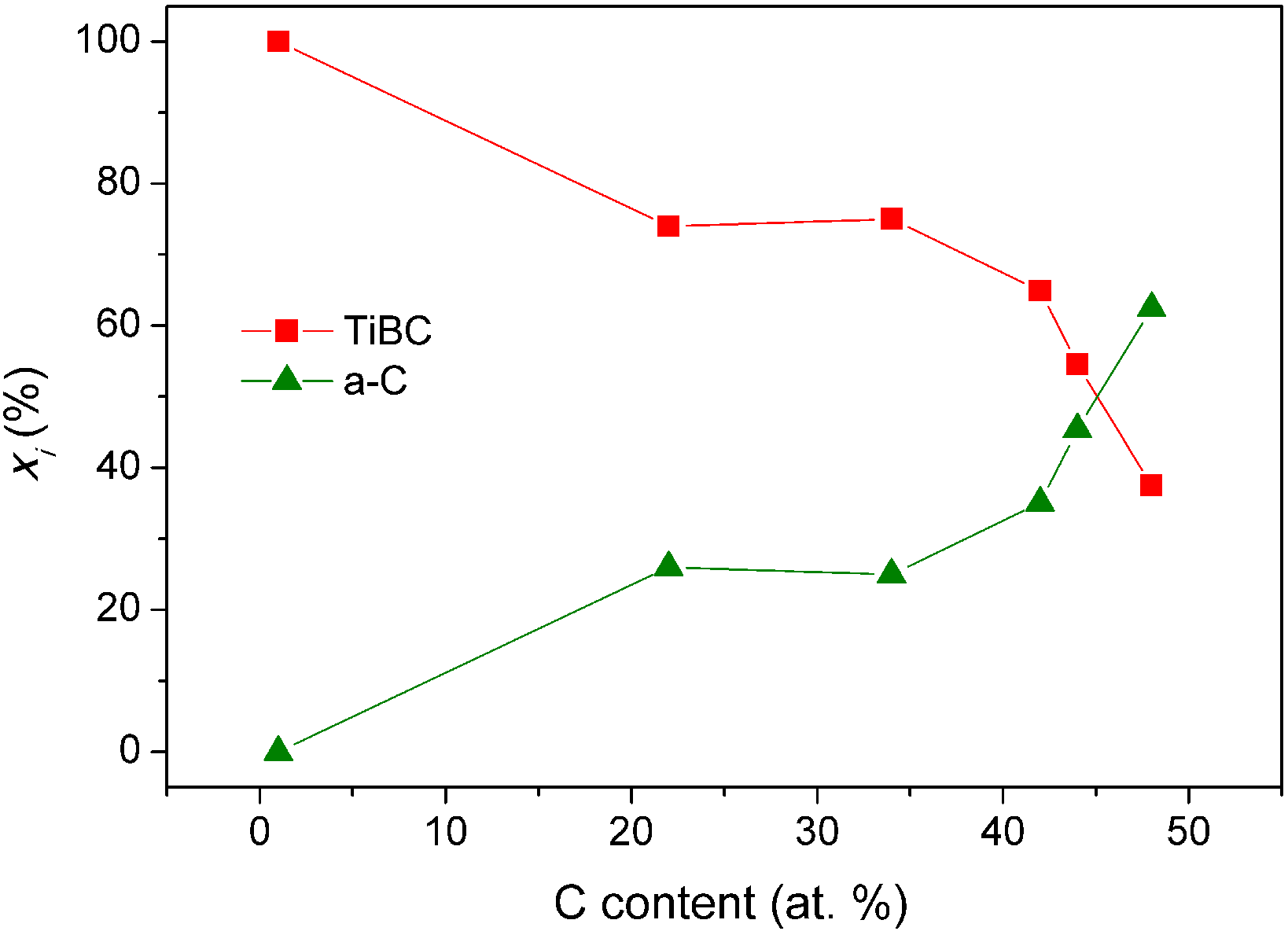
100
80
60
40
20
0
x_i (%)
TiBC
a-C
0
10
20
30
40
50
C content (at. %)

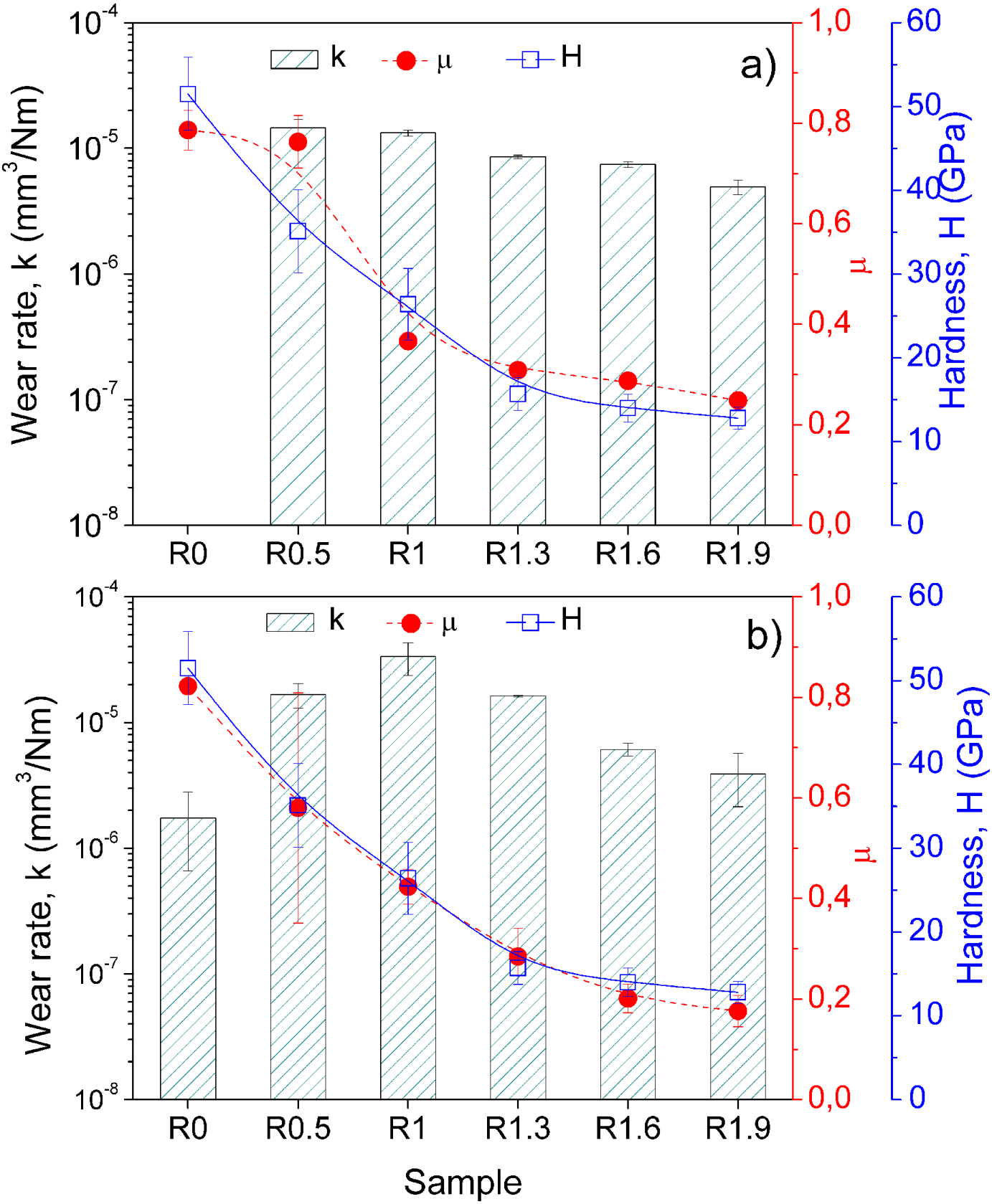
a)
b)
k
μ
H
Wear rate, k (mm³/Nm)
μ
Hardness, H (GPa)
10⁻⁴
10⁻⁵
10⁻⁶
10⁻⁷
10⁻⁸
1,0
0,8
0,6
0,4
0,2
0,0
60
50
40
30
20
10
0
R0
R0.5
R1
R1.3
R1.6
R1.9
Sample

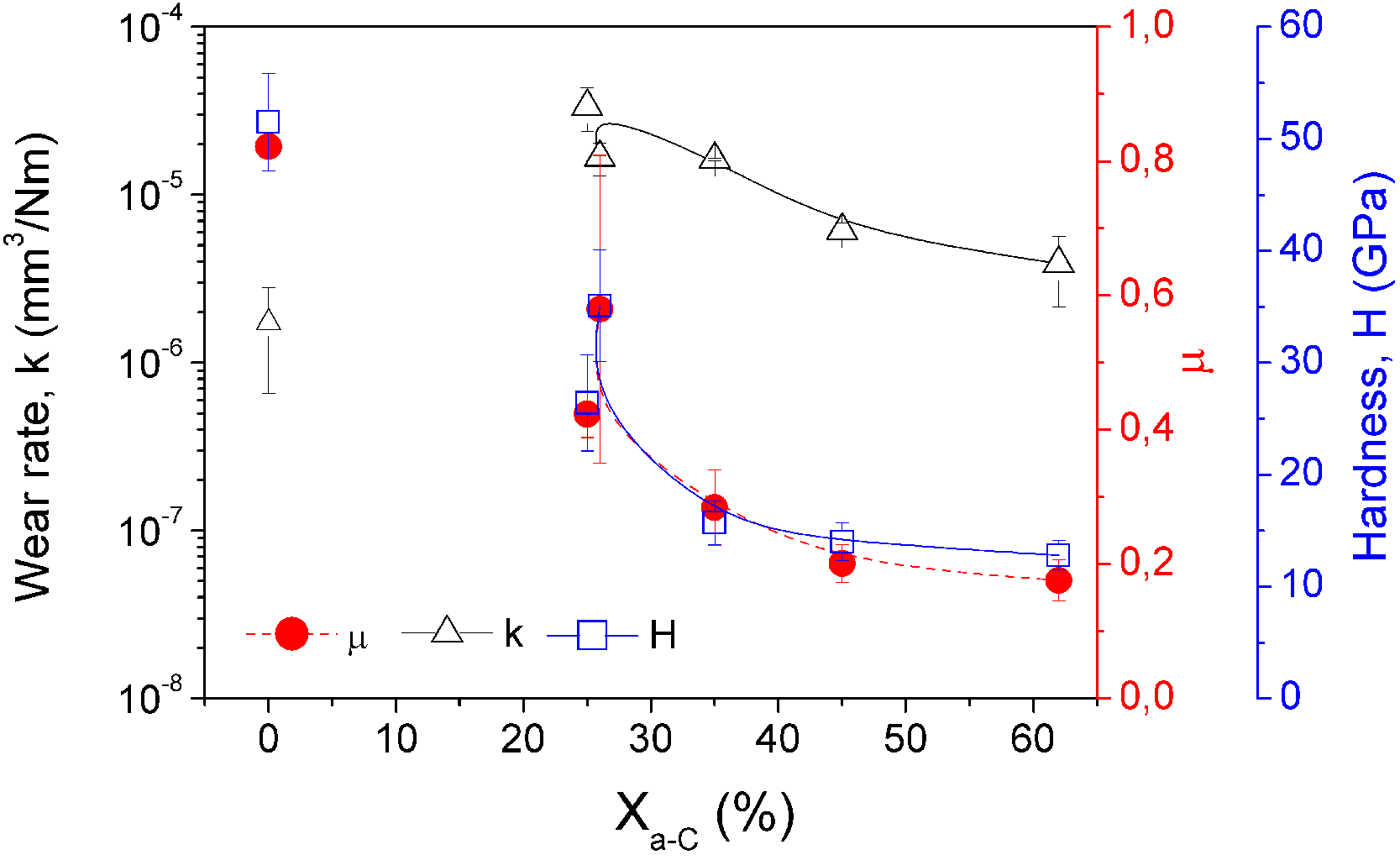
Wear rate, k (mm3/Nm)
10-4
10-5
10-6
10-7
10-8
1,0
0,8
0,6
0,4
0,2
0,0
μ
60
50
40
30
20
10
0
Hardness, H (GPa)
μ
k
H
0
10
20
30
40
50
60
Xa-C (%)

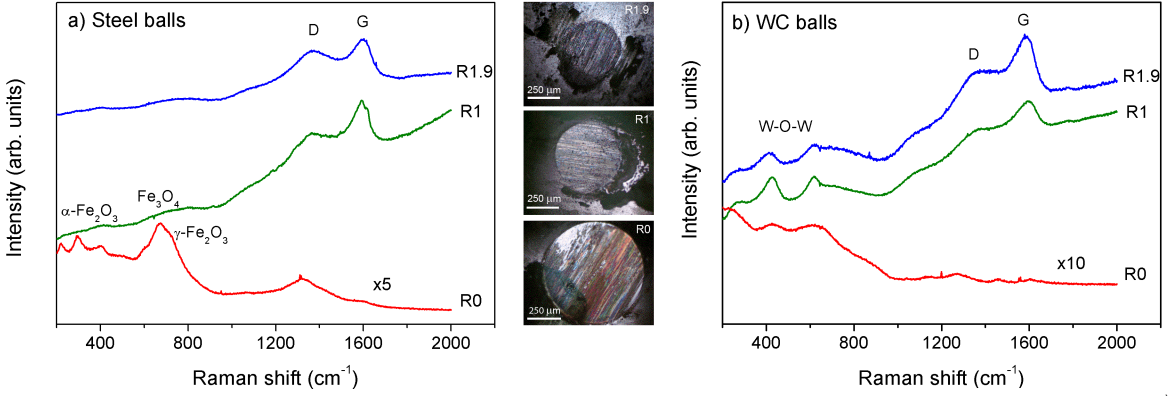
a) Steel balls
D
G
R1.9
R1
α-Fe2O3
Fe3O4
γ-Fe2O3
x5
R0
Intensity (arb. units)
400
800
1200
1600
2000
Raman shift (cm-1)
R1.9
250 μm
R1
250 μm
R0
250 μm
b) WC balls
G
D
R1.9
W-O-W
R1
x10
R0
Intensity (arb. units)
400
800
1200
1600
2000
Raman shift (cm-1)